



**HAL**  
open science

## Feasibility study of fissile mass detection in 870 L radioactive waste drums using delayed gamma rays from neutron-induced fission

R. de Stefano, C. Carasco, B. Pérot, E. Simon, T. Nicol, E. Mauerhofer

### ► To cite this version:

R. de Stefano, C. Carasco, B. Pérot, E. Simon, T. Nicol, et al.. Feasibility study of fissile mass detection in 870 L radioactive waste drums using delayed gamma rays from neutron-induced fission. *Journal of Radioanalytical and Nuclear Chemistry*, 2019, 322, pp.1185-1194. 10.1007/s10967-019-06731-2 . cea-02591079

**HAL Id: cea-02591079**

**<https://cea.hal.science/cea-02591079>**

Submitted on 15 May 2020

**HAL** is a multi-disciplinary open access archive for the deposit and dissemination of scientific research documents, whether they are published or not. The documents may come from teaching and research institutions in France or abroad, or from public or private research centers.

L'archive ouverte pluridisciplinaire **HAL**, est destinée au dépôt et à la diffusion de documents scientifiques de niveau recherche, publiés ou non, émanant des établissements d'enseignement et de recherche français ou étrangers, des laboratoires publics ou privés.



## 22        **Introduction**

23        Since the end of the '80s, CEA has produced large volume 870 L radioactive waste  
24        drums [1] that are stored in Cadarache, France. These legacy drums are filled with wafers  
25        corresponding to smaller compacted drums. The fissile mass within the drums needs to be  
26        known in order to limit criticality risks during transport, interim storage and in the final  
27        repository for which the maximum accepted fissile mass is of the order of 200 g. In  
28        practice, only tens of grams of fissile mass are really expected to be present in these  
29        drums [2]. The goal of the work presented in this paper is to test the preliminary  
30        detectability of some tens of grams of  $^{235}\text{U}$  or  $^{239}\text{Pu}$  with three different distributions in  
31        the 870 L drum by neutron-induced fission delayed gamma rays measurement.

32        The delayed gamma rays of interest emitted by the fission products of  $^{235}\text{U}$  and  $^{239}\text{Pu}$   
33        have been identified in previous work mainly presented in [2] and [13]. We select six of  
34        these delayed gamma rays for this feasibility study. These delayed gamma rays and their  
35        respective fission product and half-life based on LARA nuclear database [3] are reported  
36        in Tab. 1. The MCNP 6.1 Activation Control Card (ACT Card) [4] is used to simulate  
37        fission delayed gamma rays. As shown in more details in the work presented in [5], the  
38        ACT card correctly reproduces the order of magnitude of the experimental net counts  
39        obtained by irradiating bare samples (i.e. without waste matrix) of Highly Enriched  
40        Uranium (HEU) and Plutonium in REGAIN Prompt Gamma Neutron Activation  
41        Analysis (PGNAA) cell of the Nuclear Measurement Laboratory of CEA Cadarache,  
42        France. REGAIN was made of graphite walls, a pulsed DT neutron generator and a 33 %  
43        HPGe (high purity germanium) detector.

44        As REGAIN is today dismantled and was only able to accept 120 L waste drums, we  
45        decided to perform this feasibility study of fission delayed gamma-ray detectability in  
46        870 L legacy waste drums with the MCNP model of another PGNAA cell called  
47        MEDINA (Multi Element Detection based on Instrumental Neutron Activation), located  
48        at FZJ in Jülich, Germany. With this MEDINA model, we already studied the detection  
49        of neutron-induced fission delayed gamma rays in 225 L waste drums as reported in [6],  
50        without the ACT card. In [6], calculation was split in two steps: (1) fission rate followed

51 by (2) detection of fission delayed gamma rays. In the present study, the ACT card allows  
 52 simplifying calculation by directly obtaining the fission delayed photon flux at the  
 53 entrance of the HPGe detector. For the present work, the MCNP model of MEDINA was  
 54 adapted to accept 870 L drums. The time vs. energy output data from the MCNP  
 55 calculations (F5:P tally, i.e. photon flux at the detector position) was then processed with  
 56 MODAR Software (MCNP Output Data Analysis with Root) [7]. This last allows a  
 57 temporal analysis of gamma rays of interest and the convolution of the photon flux  
 58 spectra with the response function of a HPGe detector.

$\gamma$ ray energy	885 keV	1011 keV	1384 keV	1436 keV	1768 keV	2218 keV
Fission fragment	$^{104}\text{Tc}$	$^{101}\text{Mo}$	$^{92}\text{Sr}$	$^{138}\text{Cs}$	$^{138}\text{Xe}$	$^{138}\text{Cs}$
Half-life $T_{1/2}$	18.3 min	14.6 min	2.65 h	33.4 min	14.1 min	33.4 min

59 **Table 1.** Main delayed gamma rays emitted by  $^{235}\text{U}$  and  $^{239}\text{Pu}$  fission fragments for this  
 60 study.

### 61 **Validation of the use of MCNP 6.1 Activation Control Card**

62 The study presented in details in [5] consisted in confronting experimental results  
 63 obtained with REGAIN graphite cell with simulated results. Some of the experiments led  
 64 during the campaign presented in [6] consisted of interrogating a metallic Highly  
 65 Enriched Uranium (HEU) or plutonium bare sample of some tens of grams by 14 MeV  
 66 neutrons emitted by a GENIE 16 neutron generator of  $8.10^7 \text{ s}^{-1}$  average intensity  
 67 thermalized in the cell. The HEU and plutonium samples were irradiated for 2 h and were  
 68 then moved to a low-background spectrometer where the delayed gamma rays were  
 69 measured with a 25 % relative efficiency HPGe, with sequential spectra acquisitions  
 70 every 15 min, for a global 24-h measurement time. In the low-background cell, a thin 3  
 71 mm lead shield was placed between the fissile materials metallic samples and the HPGe  
 72 detector in order to limit the signal from the low energy gamma rays of  $^{241}\text{Am}$ . The 24-h  
 73 measurements have been simulated using the models described in [5], taking into account  
 74 the transfer of the bare samples from REGAIN cell to the low-background cell (1-min  
 75 transfer). The time chronogram of these experiments is presented in Fig. 1.

76 All gamma rays from activation of non-nuclear materials in the cell were not calculated  
 77 by using the option NONFISSION=NONE of ACT Card, thus simulating the low-  
 78 background cell conditions. The delayed gamma rays calculated with MCNP 6.1 ACT  
 79 card were studied by analyzing the decay time of non-nuclear activated elements and  
 80 fission fragments as detailed in [5]. The simulated net counts are calculated for the first  
 81 15 min after the end of irradiation by applying the formula in Eq. (1):

$$82 \quad MCNP_{counts}(E) = \int_{t_2}^{t_3} \left( \int_{E'} F5_{ACT}(E', t) \times RF_{HPGe33\%}(E', E) dE' \right) dt \cdot T_{irrad} \cdot E_n \quad (1)$$

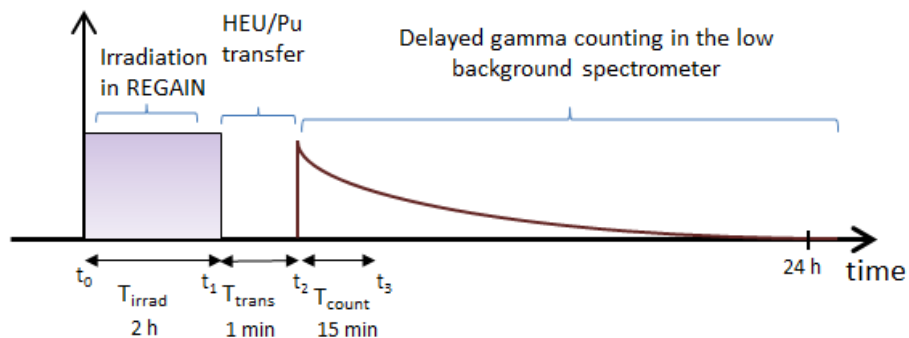
83 where  $t_2 = 1$  min is the time transfer from REGAIN to the low-background spectrometer  
 84 and  $t_3 = 16$  min ;  $F5_{ACT}(E', t)$  corresponds to the point photon flux obtained at the entrance  
 85 of the HPGe detector; The response function  $RF_{HPGe33\%}(E', E)$  corresponds to the  
 86 probability that a photon with energy  $E'$  leads to an energy deposit  $E$  in the gamma-ray  
 87 HPGe detector of 33% relative efficiency;  $T_{irrad}$  (s) is the full irradiation time of 2 hours;  
 88  $E_n$  ( $n \cdot s^{-1}$ ) is the  $8.10^7$   $n \cdot s^{-1}$  average neutron emission of the GENIE 16 neutron generator  
 89 during irradiation. In addition, as MODAR response function corresponds to a 33 %  
 90 HPGe, we have also calculated the efficiency of the 25 % HPGe used in the low-  
 91 background spectrometer and we have applied the correction reported in Tab. 2 for each  
 92 delayed gamma ray. The respective full energy peaks efficiencies are calculated with an  
 93 isotropic mono-energetic photon point source placed 12.5 cm from both 25 % and 33 %  
 94 relative efficiency HPGe detectors (like in REGAIN experiment) and a F8:P energy  
 95 deposition tally in the volume of the respective germanium crystal cells presented in Fig.  
 96 2.

97 In the MCNP net simulated counts in Tab. 3 only statistical uncertainties linked to each  
 98 computation are reported. Indeed, these numerical simulations have been performed with  
 99  $5 \times 10^9$  source neutrons, which corresponds to a relative statistical uncertainty on each  
 100 gamma ray present in the F5:P photon flux tally between 1 % and 3 %. However, this  
 101 figure does not represent the total MCNP calculation uncertainty. Indeed, the uncertainty  
 102 associated to the fine geometrical description of nuclear material metallic HEU and Pu  
 103 bare samples in the numerical model might be significant as self-shielding is large in  
 104 these samples, and extremely geometry-dependent. Calculated self-shielding factors

105 reported in ref. [6] are 3.8 and 5.7 in the HEU and Pu samples, respectively, but ref. [6]  
 106 also reports that calculation underestimates the measured fission rates by 55 % and 37 %,   
 107 respectively. This is probably due to discrepancies between the models and the real  
 108 geometry of these samples. Indeed, the geometry of the metallic fissile core of these old  
 109 samples manufactured in the '60s is not known with a good precision and only their outer  
 110 dimensions (of the zirconium alloy envelope) and masses are well known. In addition, the  
 111 uncertainties on nuclear data, in particular on fission products yields (leading to delayed  
 112 gamma ray emissions) are not taken into account. Concerning experimental results  
 113 reported in Tab. 3, the standard deviation on the net peak area S (number of counts) of a  
 114 delayed gamma ray is calculated with Eq. 2 (following Poisson law).

$$115 \quad \sigma = \sqrt{S + 2B} \quad (2)$$

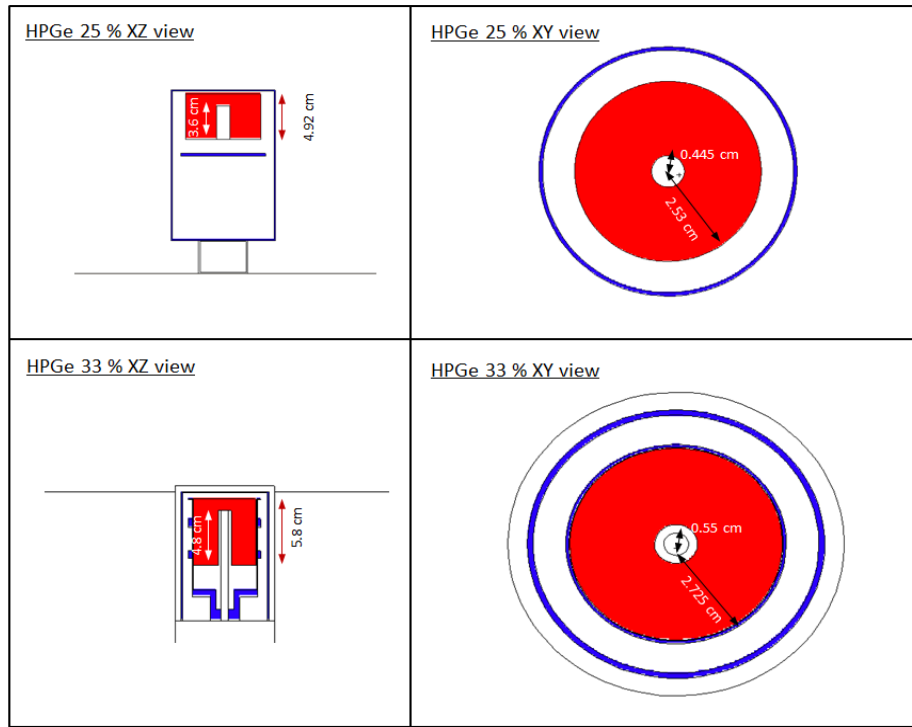
116 where B is the Compton continuum background under the peak (number of counts). For  
 117 the main experimental results  $\sigma$  corresponds to an experimental relative uncertainty of  
 118 about 10 %, which is much smaller than the uncertainties related to self-shielding which  
 119 are described above. Calculations and measurements being of the same order of  
 120 magnitude is however encouraging enough to allow further numerical exploratory  
 121 investigations using MCNP 6.1 ACT card. Consequently, we will use this delayed  
 122 gamma-ray calculations method based on MCNP ACT card to study the feasibility of the  
 123 870 L drum characterization by the measurement of delayed gamma rays from neutron-  
 124 induced fission.



125

126 **Fig 1:** Time chronogram related to the HEU/Pu samples irradiation in REGAIN and  
 127 delayed gamma measurement in the low-background spectrometer

128



129

130 Fig. 2 MCNP models of the 33 % and 25 % relative efficiencies HPGe detectors with  
 131 their respective germanium crystals (red) and aluminum envelopes (blue). Note that the  
 132 XZ and XY views are not at the same scale.

$\gamma$ ray energy	885 keV	1011 keV	1384 keV	1436 keV	1768 keV	2218 keV
Efficiency for a HPGe 25%	$1.471 \times 10^{-3}$	$1.334 \times 10^{-3}$	$1.014 \times 10^{-3}$	$0.982 \times 10^{-3}$	$0.820 \times 10^{-3}$	$6.582 \times 10^{-4}$
Efficiency for a HPGe 33%	$1.875 \times 10^{-3}$	$1.686 \times 10^{-3}$	$1.317 \times 10^{-3}$	$1.277 \times 10^{-3}$	$1.054 \times 10^{-3}$	$0.880 \times 10^{-3}$
Correction factor	<b>0.784</b>	<b>0.791</b>	<b>0.770</b>	<b>0.769</b>	<b>0.778</b>	<b>0.748</b>

133 Table 2. Detection efficiencies of the 33 % and 25 % HPGe detectors calculated with  
 134 MCNP (see models in Fig. 2) for a gamma point source located at 12.5 cm from the  
 135 detector entrance surfaces as in the experiment.

136

$\gamma$ ray energy	885 keV	1011 keV	1384 keV	1436 keV	1768 keV	2218 keV
Experimental net counts with U	$790 \pm 67$	$918 \pm 98$	$612 \pm 40$	$1211 \pm 54$	$172 \pm 25$	$102 \pm 24$
MCNP 6.1 net counts with U	$648 \pm 8$	$744 \pm 23$	$597 \pm 10$	$877 \pm 12$	$183 \pm 4$	$130 \pm 3$
Experimental net counts with Pu	$1464 \pm 106$	$760 \pm 66$	$347 \pm 36$	$1057 \pm 48$	$102 \pm 29$	$198 \pm 37$
MCNP 6.1 net counts with Pu	$873 \pm 6$	$552 \pm 14$	$238 \pm 3$	$567 \pm 4$	$118 \pm 2$	$85 \pm 1$

137 **Table 3** Simulated net counts vs. experimental net counts of the main delayed gamma  
138 rays of interest from HEU and plutonium samples after a 15-min measurement following  
139 a 2-h irradiation in the REGAIN neutron interrogation cell.

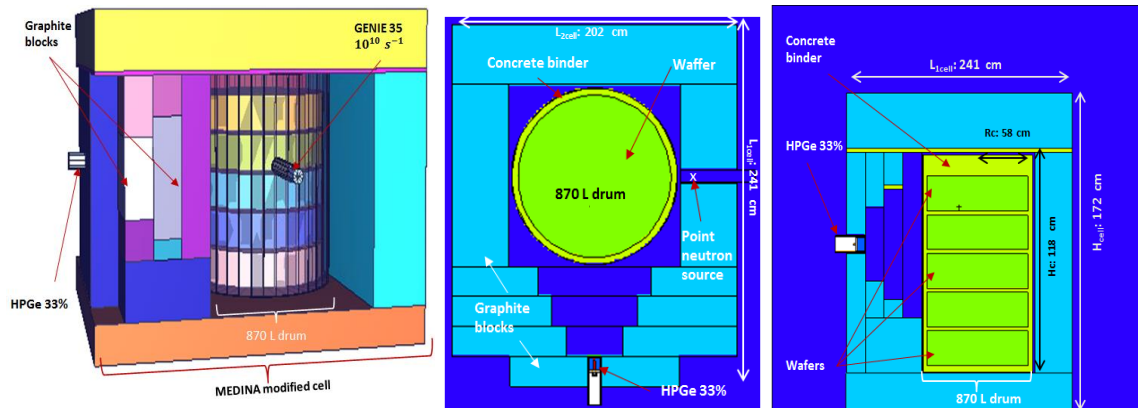
#### 140 **MCNP model of the measurement cell for the 870 L drums**

141 The graphite cell used for this study is based on an existing MCNP model of the  
142 MEDINA facility of the Forschungszentrum Jülich (FZJ) described in [6] [8] [9]. As  
143 MEDINA was built with the aim of detecting toxic chemicals in up to 225 L drums the  
144 model of this MEDINA cell has been slightly modified by enlarging the interrogation  
145 cavity to accept the 870 L waste drum. A graphite block has also been added in the  
146 bottom of the cell to limit neutron leakages to the ground. In the same way, the graphite  
147 roof of the cell has been enlarged to limit neutron leakage in the top corners of the cell  
148 and thus improve the thermal neutron flux and hence fissile mass interrogation. The new  
149 model of the cell named MEDINA 2 is presented in Fig. 3.

150 As MEDINA cell, MEDINA 2 is modelled with high purity graphite blocks allowing the  
151 14 MeV fast neutron thermalisation. The composition of this graphite blocks used for this  
152 model is reported in Tab. 4. An isotropic 14 MeV neutron point source is simulated with  
153 a  $10^{10} \text{ s}^{-1}$  intensity (corresponding to a GENIE 35 neutron generator of SODERN). Note  
154 that the original 104 % relative efficiency HPGe of MEDINA is replaced by a 33 %  
155 HPGe, the response function of this detector being available in MODAR for time-energy  
156 investigations. For the first study, 10 g of  $^{235}\text{U}$  or  $^{239}\text{Pu}$  were simulated with a

157 homogenous distribution in the five compacted drums filling the 870 L drum, meaning 2  
 158 g per wafer. The detailed description of the 870 L drum geometry and materials is given  
 159 in [2]. For the second and third case studies corresponding to heterogeneous fissile  
 160 materials, two metallic 10 g  $^{235}\text{U}$  and  $^{239}\text{Pu}$  spheres (radius  $\approx 0.5$  cm) were simulated at  
 161 the edge and in the center of the third wafer. Spheric shapes are chosen as simplification,  
 162 in order to avoid anisotropic self-attenuation effects within the sample.

163



164

165 **Fig. 3.** 3D view (left), horizontal cross section (middle) and vertical cross section (right)  
 166 of the MEDINA 2 graphite cell with a 870 L drum.

167

168

169

170

171

172

173

Element	% Weight	Element	% Weight	Element	% Weight
<sup>12</sup> C	99.913	<sup>1</sup> H	$4.05 \times 10^{-3}$	<sup>46</sup> Ti	$3.28 \times 10^{-4}$
<sup>40</sup> Ca	$1.09 \times 10^{-2}$	<sup>54</sup> Fe	$2.93 \times 10^{-4}$	<sup>47</sup> Ti	$2.99 \times 10^{-4}$
<sup>42</sup> Ca	$1.27 \times 10^{-4}$	<sup>56</sup> Fe	$4.59 \times 10^{-3}$	<sup>48</sup> Ti	$3.03 \times 10^{-4}$
<sup>43</sup> Ca	$2.73 \times 10^{-5}$	<sup>57</sup> Fe	$1.10 \times 10^{-4}$	<sup>49</sup> Ti	$2.26 \times 10^{-4}$
<sup>44</sup> Ca	$5.58 \times 10^{-4}$	<sup>58</sup> Fe	$1.40 \times 10^{-5}$	<sup>50</sup> Ti	$2.21 \times 10^{-4}$
<sup>48</sup> Ca	$3.71 \times 10^{-4}$	<sup>35</sup> Cl	$1.52 \times 10^{-4}$	<sup>10</sup> B	$3.70 \times 10^{-5}$
<sup>32</sup> P	$1.09 \times 10^{-2}$	<sup>37</sup> Cl	$4.87 \times 10^{-5}$	<sup>11</sup> B	$1.49 \times 10^{-4}$
<sup>33</sup> P	$8.63 \times 10^{-5}$	<sup>51</sup> V	$3.50 \times 10^{-4}$		
<sup>34</sup> P	$4.84 \times 10^{-4}$	<sup>27</sup> Al	$4.05 \times 10^{-2}$		

174 Table 4: Graphite blocks composition for the model of the MEDINA2 measurement cell  
 175 for the 870 L drums

## 176 MCNP calculations for a homogeneous distribution of fissile materials

177 The delayed gamma ray spectra emitted by 10 g of fissile masses homogeneously  
 178 distributed in the five compacted drums are shown in Fig. 4 for both <sup>235</sup>U and <sup>239</sup>Pu. The  
 179 main high energy delayed gamma rays of interest from uranium and plutonium (reported  
 180 in Tab. 1) are present in both spectra. With the aim of being closer to realistic practical  
 181 measurement of these drums, the net number of counts in these peaks has been simulated  
 182 for a 3-h acquisition time following the end of the 2-h irradiation, see Tab. 5. The MCNP  
 183 net number of counts for this study are calculated following Eq. (1) with  $t_2 = 1$  min and  
 184  $t_3 = 3$  hours.

185 Tab. 5 reports statistical uncertainties on the net peak area (number of counts S after  
 186 subtraction of the Compton continuum background B in the HPGe gamma spectrum

187 simulated with MCNP) of the delayed gamma rays of interest, calculated following Eq.  
188 (2).

189 In addition, in order to calculate detection limits, the active background spectrum  
190 corresponding to the activation of the 870 L waste package materials with the  
191 NONFISSION = P option of the ACT card has been calculated. The same conditions as  
192 for the fission delayed gamma ray useful signal have been used (neutron generator  
193 emission, irradiation and counting time). The calculated activation background spectrum  
194 reported in Fig. 5 shows no interference between delayed gamma rays of interest for this  
195 study and activation gamma rays from the 870 L waste drum. However, the useful signal  
196 spectrum of fission delayed gamma rays is 1 to 2 orders of magnitude smaller than the  
197 active background spectrum (see Fig. 4 vs. Fig. 5, respectively). Detection Limits (DL in  
198 counts) are calculated following Eq. (3), which corresponds to a non-detection risk and a  
199 false-alarm risk  $\alpha=2.5\%$  and  $\beta=2.5\%$ , respectively [10]:

$$200 \quad DL(E) \approx 3,92 \cdot \sqrt{2 \cdot B_{active\ background}(E)} \quad (3)$$

201 where  $B_{active\ background}(E)$  corresponds to Compton continuum (counts) of the active  
202 background spectrum evaluated in the region of interest of each fission delayed gamma  
203 ray (energy E), the width of which is between 7 and 8 keV depending on the peak. DL is  
204 then divided by the useful signal sensitivity, noted  $S_{U/Pu}$  (in  $g^{-1}$ ), which corresponds to the  
205 net counts reported in Tab. 5 per fissile mass unit (U or Pu). The number of counts for the  
206 870 L drum active background continuum and the detection limits in grams for a fissile  
207 mass homogeneous distribution in the 5 wafers of the 870 L drum are reported in Tab. 6.

208 For this 2-h irradiation and 3-h measurement, depending on the delayed gamma ray of  
209 interest, detection limits vary between 31.6 g and 123.4 g of  $^{235}U$ , or between 24.1 g and  
210 109.7 g of  $^{239}Pu$  homogeneously distributed in the drum.

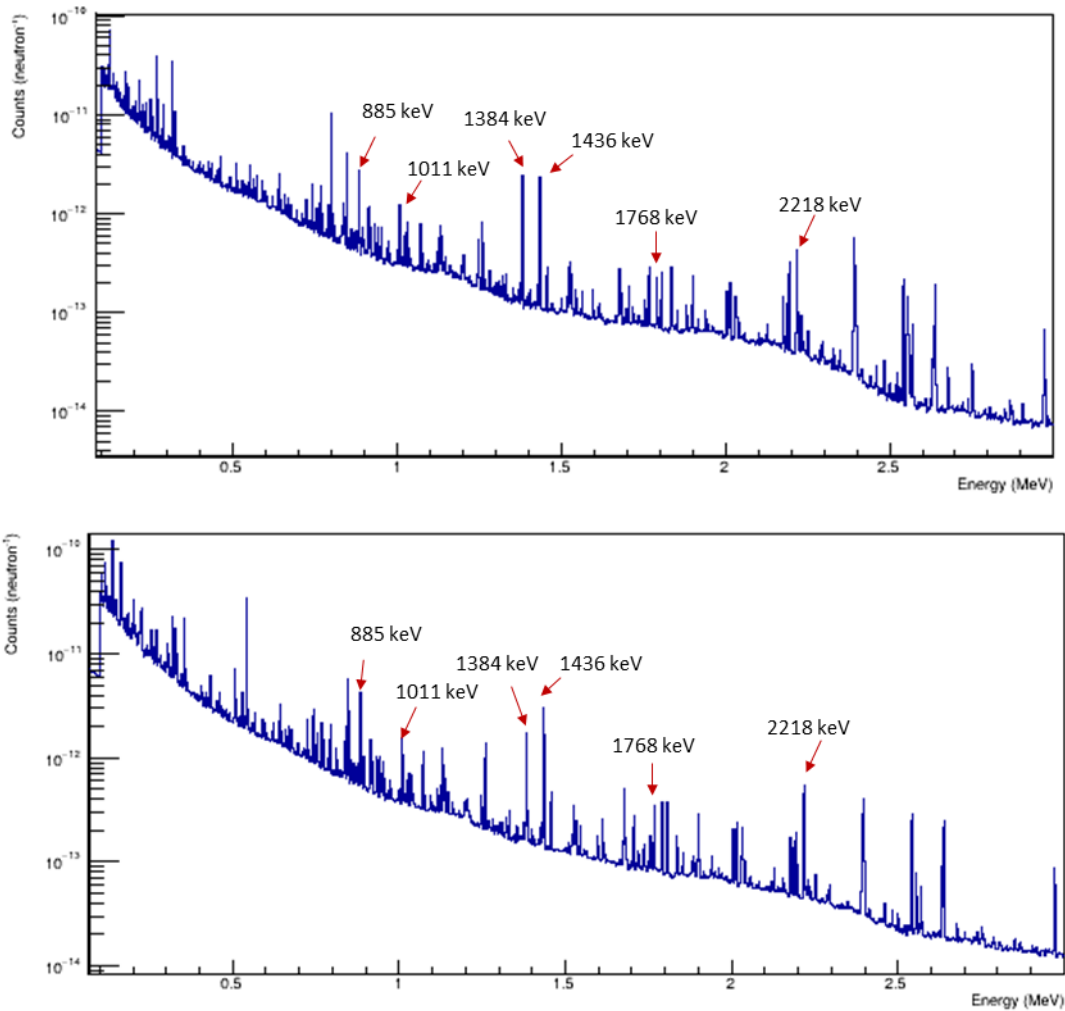
211

212

213

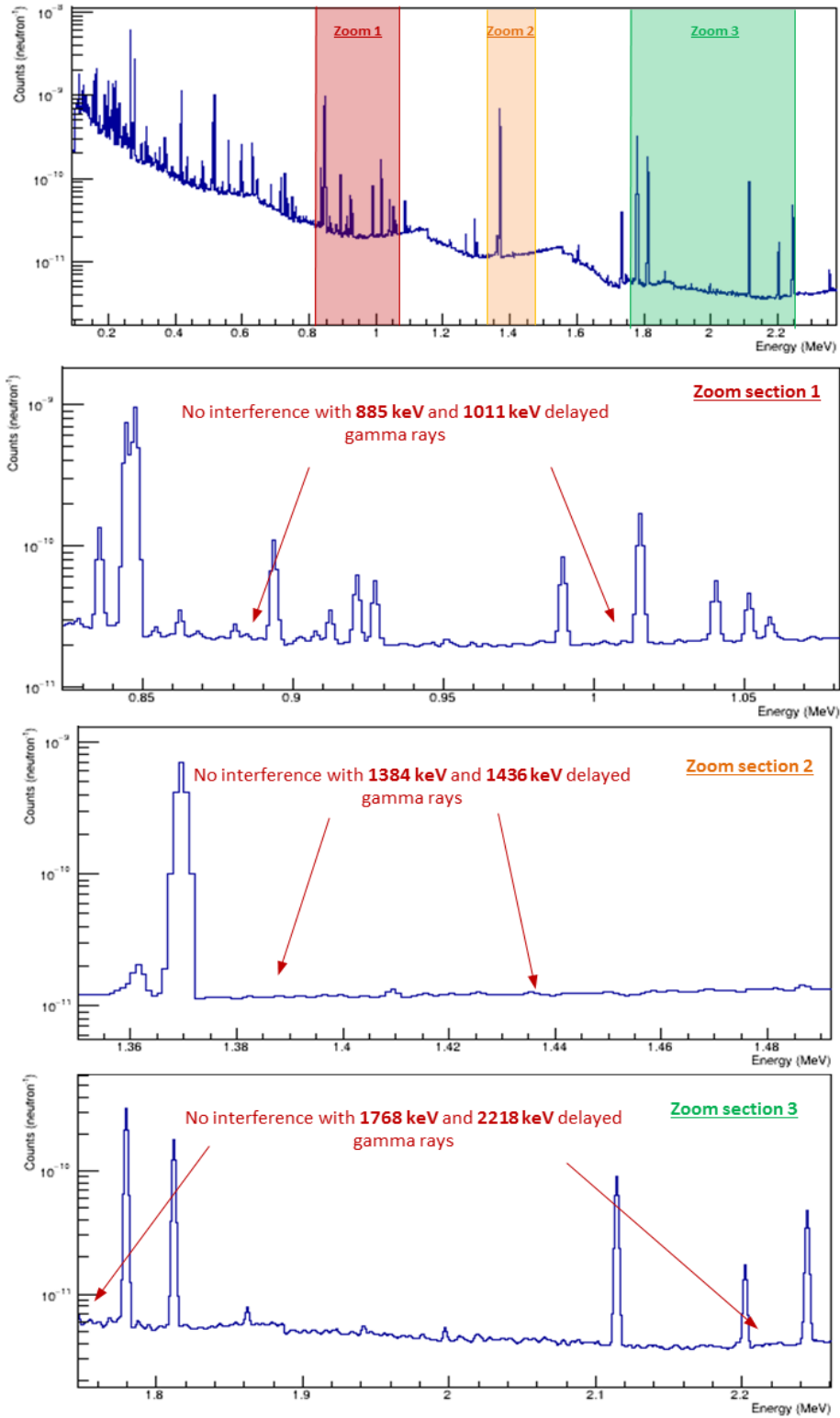
$\gamma$ ray energy	885 keV	1011 keV	1384 keV	1436 keV	1768 keV	2218 keV
Net area for $^{235}\text{U}$ (counts)	$397 \pm 24$	$265 \pm 19$	$308 \pm 22$	$395 \pm 23$	$83 \pm 11$	$90 \pm 12$
Net area for $^{239}\text{Pu}$ (counts)	$656 \pm 39$	$412 \pm 33$	$280 \pm 23$	$524 \pm 26$	$90 \pm 11$	$102 \pm 11$

214 **Table 5** Net counts in the main fission delayed gamma rays calculated with MCNP for a  
 215 3-h measurement after the end of the 2-h neutron irradiation, for 10 g of  $^{235}\text{U}$  and  $^{239}\text{Pu}$   
 216 homogeneously distributed in the 870 L drum.



217

218 **Fig. 4** MCNP simulated spectra obtained for a 3-h measurement after a 2-h irradiation of  
 219 a 870 L drum containing 10 g of homogenous distributed  $^{235}\text{U}$  (above) and  $^{239}\text{Pu}$   
 220 (below).



221

222

223

224

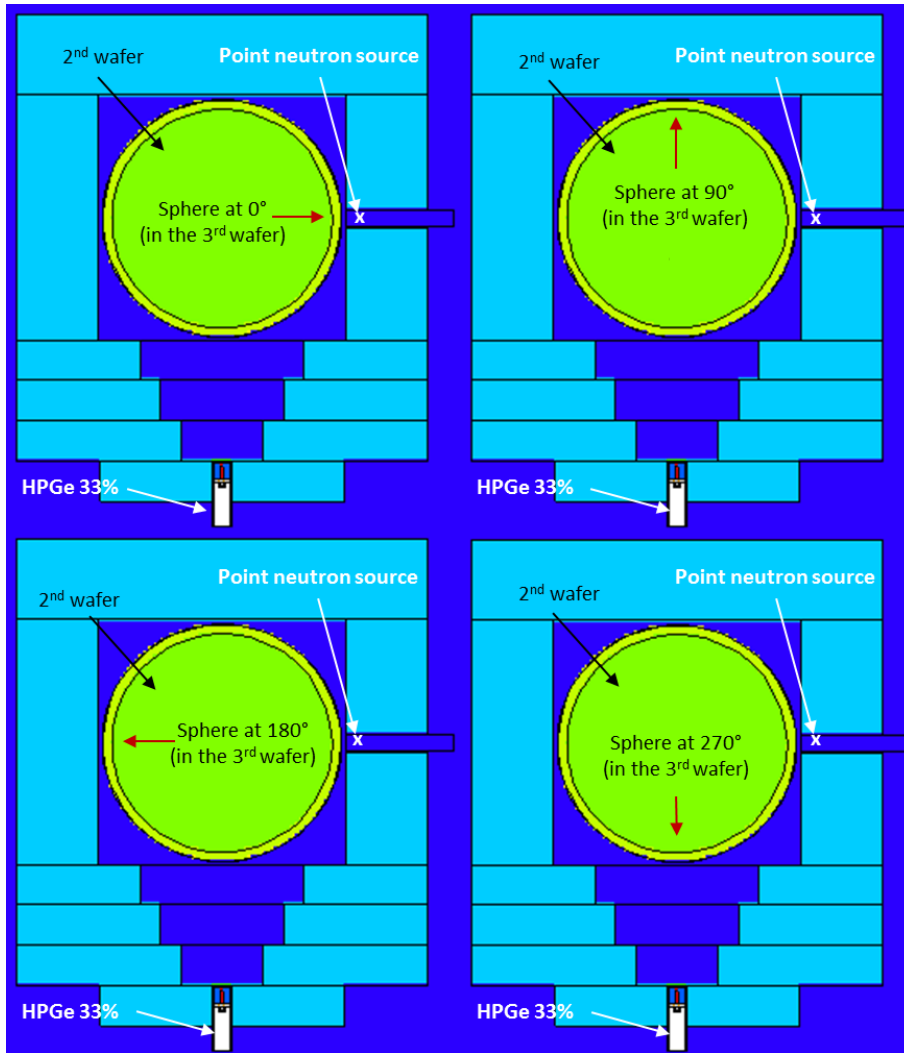
**Fig. 5** Simulated active background spectra for a 3-h measurement with a HPGe of 33 % relative efficiency detector after a 2-h irradiation of a 870 L drum, and corresponding zoom sections

$\gamma$ ray energy	885 keV	1011 keV	1384 keV	1436 keV	1768 keV	2218 keV
DL (in counts)	1928	1882	1457	1262	987	729
DL in $^{235}\text{U}$ mass (g)	48.2	69.7	47.0	31.6	123.4	81.0
DL in $^{239}\text{Pu}$ mass (g)	29.4	45.7	52.0	24.1	109.7	71.5

225 **Table 6** Detection limits of  $^{235}\text{U}$  and  $^{239}\text{Pu}$  homogeneously distributed in the 870 L drum  
 226 for each delayed gamma ray of interest.

### 227 **MCNP calculations for a peripheral distribution of fissile materials**

228 The second study corresponds to a 10 g sphere of  $^{235}\text{U}$  or  $^{239}\text{Pu}$  located in a peripheral  
 229 position, i.e. 1 cm from the edge of the third middle wafer. Four positions with respect to  
 230 neutron generator and detector have been studied:  $0^\circ$ ,  $90^\circ$ ,  $180^\circ$  and  $270^\circ$  as shown in  
 231 Fig. 6. The results obtained for 10 g of  $^{235}\text{U}$  or  $^{239}\text{Pu}$  placed at the edge of the drum are  
 232 reported in Tab. 7 and Tab. 8, respectively. For each angle, irradiation time is 2 h. The  
 233 net counts obtained for both uranium and plutonium in  $0^\circ$  and  $270^\circ$  positions are much  
 234 smaller than with a homogenous distribution, and the signal is not detectable in the  $90^\circ$   
 235 and  $180^\circ$  positions. This is mainly due to neutron self-shielding and gamma self-  
 236 absorption inside the thick nuclear material spheres (1 cm in diameter), and to  
 237 combined matrix-position effects leading also to large neutron and gamma attenuation in  
 238 the 870 L waste materials. Detection limits have also been estimated following Eq. (3) for  
 239 a peripheral distribution at  $0^\circ$  and  $270^\circ$  with respect to the neutron generator, and are  
 240 reported in Tab. 9. Detection limits are too high (dozens or hundreds of grams) to  
 241 envisage a practical application of the method for these drums.



242

243 **Fig. 6** XY view of MEDINA 2 cell and the 870 L drum with a 10 g fissile material sphere  
 244 placed at the following irradiation angles with respect to neutron generator: 0°, 90°, 180°  
 245 and 270°.

$\gamma$ ray energy	885 keV	1011 keV	1384 keV	1436 keV	1768 keV	2218 keV
Net area at 0° (counts)	39 ± 11	60 ± 9	74 ± 11	64 ± 10	13 ± 5	14 ± 5
Net area at 90° (counts)	< 1	< 1	< 1	< 1	< 1	< 1
Net area at 180° (counts)	< 1	< 1	< 1	< 1	< 1	< 1
Net area at 270° (counts)	145 ± 16	115 ± 12	126 ± 14	167 ± 18	30 ± 7	31 ± 7

246 **Table 7** Net counts for a 3-h measurement after the end of the 2-h neutron irradiation for  
 247 the main delayed gamma rays of 10 g of <sup>235</sup>U placed at the edge of the 870 L drum.

248

$\gamma$ ray energy	885 keV	1011 keV	1384 keV	1436 keV	1768 keV	2218 keV
Net area at 0° (counts)	188 ± 33	77 ± 20	72 ± 11	90 ± 12	20 ± 5	22 ± 5
Net area at 90° (counts)	< 1	< 1	< 1	< 1	< 1	< 1
Net area at 180° (counts)	< 1	< 1	< 1	< 1	< 1	< 1
Net area at 270° (counts)	233 ± 25	128 ± 17	122 ± 13	161 ± 14	25 ± 6	30 ± 6

249 **Table 8** Net counts for a 3-h measurement after the end of the 2-h neutron irradiation for  
 250 the main delayed gamma rays of 10 g of  $^{239}\text{Pu}$  placed at the edge of the 870 L drum.

251

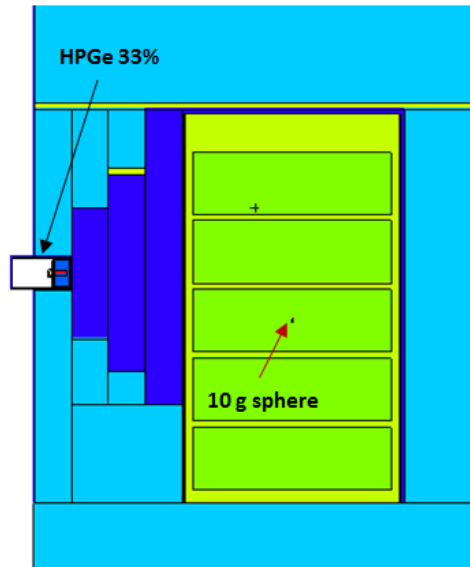
$\gamma$ ray energy	885 keV	1011 keV	1384 keV	1436 keV	1768 keV	2218 keV
DL in $^{235}\text{U}$ mass (g) at 0°	494	313	197	197	760	520
DL in $^{239}\text{Pu}$ mass (g) at 0°	102	250	202	140	494	331
DL in $^{235}\text{U}$ mass (g) at 270°	133	164	115	76	329	235
DL in $^{239}\text{Pu}$ mass (g) at 270°	83	147	119	78	394	243

252 **Table 9** Detection limits (grams) of  $^{235}\text{U}$  and  $^{239}\text{Pu}$  located in the 870 L drum at 0° and  
 253 270° with respect to the neutron generator, for each delayed gamma ray of interest.

### 254 **MCNP calculations with fissile materials in the drum center**

255 The third case study consists of fissile material placed in the drum center, in the middle  
 256 of the third wafer as shown in Fig. 7. The results obtained for a 2 h drum irradiation  
 257 followed by a 3 h counting measurement for the  $^{235}\text{U}$  and  $^{239}\text{Pu}$  spheres are reported in  
 258 Tab. 10. In this configuration, for each high energy delayed gamma ray of interest from  
 259 uranium and plutonium, the net number of counts is lower than 10 and it is clear that  
 260 detecting 10 g of fissile masses in the center of a 870 L drum is not possible. Note that  
 261 detection limits have not been calculated for this section as the net counts signal from  
 262 delayed gamma rays of interest is hardly detectable. Indeed, the performances of the  
 263 method are intrinsically very poor due to the attenuation of the interrogating neutron flux

264 in the concrete envelope of the 870 L drum. Therefore, another method based on delayed  
 265 gamma rays induced by photo-fission with high energy X-rays (produced by a 15 MeV  
 266 electron LINAC) is also currently under study at CEA, which shows more encouraging  
 267 results for nuclear materials detection in 870 L waste drums [2] [11] [12].



268

269 **Fig. 7** Vertical cross section of MEDINA 2 cell showing the 870 L drum with a 10 g  
 270 fissile material sphere placed in the center.

$\gamma$ ray energy	885 keV	1011 keV	1384 keV	1436 keV	1768 keV	2218 keV
Net area for $^{235}\text{U}$ (counts)	$3 \pm 2$	$2 \pm 1$	$7 \pm 4$	$2 \pm 1$	$2 \pm 1$	$2 \pm 1$
Net area for $^{239}\text{Pu}$ (counts)	$7 \pm 4$	$5 \pm 3$	$5 \pm 3$	$7 \pm 3$	$1 \pm 1$	$2 \pm 1$

271 **Table 10** Net counts in the main fission delayed gamma rays, for a 3-h measurement  
 272 after the end of the 2-h neutron irradiation, for 10 g of  $^{235}\text{U}$  and  $^{239}\text{Pu}$  placed at the 870 L  
 273 drum center.

274 **Conclusion and prospects**

275 This feasibility study explored the detectability of  $^{235}\text{U}$  or  $^{239}\text{Pu}$  in 870 L legacy CEA  
 276 drums by means of neutron activation analysis and neutron-induced fission delayed  
 277 gamma measurements. For this purpose, a graphite cell has been modeled with MCNP  
 278 6.1 and the net counts in the main delayed gamma rays of interest have been calculated

279 for different fissile masses distributions, for a 3-h measurement with an HPGe detector of  
280 33 % relative efficiency following a 2-h irradiation with a neutron source of  $10^{10} \text{ s}^{-1}$ .  
281 Results are encouraging for fissile materials homogeneously distributed in the waste, with  
282 detection limits between 31.6 and 123.4 grams of  $^{235}\text{U}$ , or between 24.1 and 109.7 grams  
283 of  $^{239}\text{Pu}$  for the main high energy delayed gamma rays of interest. However, in case of  
284 small samples of fissile materials located in periphery of the drum, the net counts are  
285 much smaller due to both self-shielding and combined matrix-position effects and  
286 detection limits are too high for a practical application to 870 L drums. Finally, if the  
287 samples are located in the center of the drum, it is effectively impossible to detect any  
288 delayed gamma ray of interest.

289 The signal could be increased by using a detector with higher efficiency, such as the  
290 104 % HPGe detector used in MEDINA cell [6], and by implementing several HPGe  
291 detectors around the 870 L drum. The acquisition could also be performed between the  
292 pulses of the neutron generator (instead of after irradiation only) to increase the delayed  
293 gamma counting time.

## 294 **References**

- 295 1. Inventaire national des matières et déchets radioactifs – Catalogue descriptif des  
296 familles Andra (2015).[https://www.andra.fr/download/site-principal/document/](https://www.andra.fr/download/site-principal/document/editions/559.pdf)  
297 [editions/559.pdf](https://www.andra.fr/download/site-principal/document/editions/559.pdf). Accessed 09 Apr. 2019  
298
- 299 2. E. Simon et. al. (2016) Feasibility study of fissile mass quantification by photofission  
300 delayed gamma rays in radioactive waste packages using MCNPX, Nucl. Instr. Meth.  
301 A, 840:28-35, déc. 2016.  
302
- 303 3. “NUCLEIDE-LARA on the web (2018)” [online] available on:  
304 <http://www.nucleide.org/Laraweb/index.php>  
305

- 306 4. J. W. Durkee (2012) MCNP6 Delayed-Particle Verification And Validation Rev 5,  
307 LA-UR-12-00676  
308
- 309 5. R. De Stefano et. al. (2019), Simulation of U/Pu induced fission delayed gamma rays  
310 with MCNP 6, To be published in Nuclear instrumentation and measurement methods  
311 in nuclear environments conference records (ANIMMA), June 2019.  
312
- 313 6. T. Nicol et al. (2016), Feasibility study of  $^{235}\text{U}$  and  $^{239}\text{Pu}$  characterization in  
314 radioactive waste drums using neutron-induced fission delayed gamma rays », Nucl.  
315 Instr.. Meth. Phys. A, 832:85-94.  
316
- 317 7. C. Carasco (2010) MCNP output data analysis with ROOT (MODAR) », Comp. Phys.  
318 Com., v181:2210-2211.  
319
- 320 8. T. Nicol, et. al. (2016) HPGe-detector shielding optimization with MCNP for the  
321 MEDINA neutron activation cell, J Radioannal Nucl Chem 310:865-874.  
322
- 323 9. T. Nicol et al. (2016), Quantitative comparison between PGNAA measurements and  
324 MCNPX simulations », J Radioannal Nucl Chem. 308:671-677.  
325
- 326 10. G. Gilmore, Practical Gamma-ray Spectroscopy, second edition, Wiley, 2008.  
327
- 328 11. F. Carrel et al. (2010), Identification and Differentiation of Actinides Inside Nuclear  
329 Waste Packages by Measurement of Delayed Gammas, IEEE Trans. Nucl. Sci.,  
330 57:2862-2871.  
331
- 332 12. E. Simon et. al. (2016) Fissile mass quantification in radioactive waste packages  
333 using photofission delayed gamma rays, IEEE Nucl. Sci. Symp., Med. Imag. Conf.  
334 and Room-Temp. Semicond. Det. Workshop (NSS/MIC/RTSD), 1-4  
335

- 336 13. F. Carrel et al. (2011) New Experimental Results on the Cumulative Yields From  
337 Thermal Fission of  $^{235}\text{U}$  and  $^{239}\text{Pu}$  and From Photofission of  $^{235}\text{U}$  and  $^{238}\text{U}$  Induced by  
338 Bremsstrahlung, IEEE Trans. Nucl. Sci., 58:2064-2072.